Journal of Power Sources 243 (2013) 594–602

Contents lists available at SciVerse ScienceDirect

Journal of Power Sources

journal homepage: www.elsevier.com/locate/jpowsour

Electrophoretic fabrication and pseudocapacitive properties of graphene/manganese oxide/carbon nanotube nanocomposites

Chung Jung Hung [a], Pang Lin [a], Tseung Yuen Tseng [b,*]

[a] Department of Materials Science and Engineering, National Chiao Tung University, Hsinchu 300, Taiwan
[b] Department of Electronics Engineering and Institute of Electronics, National Chiao Tung University, Hsinchu 300, Taiwan

HIGHLIGHTS

- This study provided an improvement on electrochemical performance for pseudocapacitor.
- The electrode is about 83.3% of the initial capacitance (415 F g^{-1}) after 15,000 cycles.
- The pseudocapacitor electrode exhibits high potential for practical applications.

ARTICLE INFO

Article history:
Received 8 March 2013
Received in revised form
10 June 2013
Accepted 11 June 2013
Available online 20 June 2013

Keywords:
Pseudocapacitor
Electrophoretic deposition (EPD)
Nanocomposites
Manganese oxide
Graphene
Energy storage

ABSTRACT

Hybrid nanocomposites provided a synergistic improvement on electrochemical performance and stability for pseudocapacitor. Designed graphene/carbon nanotubes (CNTs)/MnO_2 nanocomposites with CNTs electrode (in short, GMC + C) with highly nanoporous framework surface structure are fabricated by a modified electrophoretic deposition (EPD) method. Scanning electron microscopy and transmission electron microscopy analysis demonstrate that the flake-like MnO_2 thickness (about less than 10 nm) and uniformly distributed on the porous graphene/CNTs framework. X-ray diffraction shows the formation of birnessite-type MnO_2. Pseudocapacitances of the GMC + C electrode calculated by cyclic voltammetry having different scan rates of 5, 20, 50, 100, and 300 mV s^{-1} exhibit high specific capacitances of 481, 436, 413, 398, and 372 F g^{-1}, respectively. Sodium ion diffusion coefficients of the GMC + C electrode show a higher intercalation value of 3.647×10^{-8} cm^2 s^{-1} and deintercalation value of 2.899×10^{-8} cm^2 s^{-1} using chronoamperometry. Moreover, the GMC + C electrode maintains a high specific capacitance of 346 F g^{-1}, and is about 83.3% of the initial capacitance after 15,000 charge/discharge cycles. The designed hybrid GMC + C nanocomposites pseudocapacitor electrode using EPD route with the high specific capacitance, fast reaction rate, and high stability, exhibits high potential for practical applications.

1. Introduction

Development of high-performance energy storage systems has sparked interest because of the environmental issues and the decreasing availability of fossil fuels. Nowadays, pseudocapacitor, also known as electrochemical capacitor or supercapacitor, based on pseudocapacitance is regarded as one of the most promising energy storage devices because of their higher power densities than that of accumulator batteries, higher energy density as compared to traditional capacitors, high rate capability, fast charging/discharging rate, excellent cycle stability, and long cycle life [1–3].

Recently, manganese oxide (MnO_2) has been widely investigated as a promising pseudocapacitive material because of its low cost, high electrochemical activity and more friendly environmental nature than other transition metal oxides. However, the poor electrical conductivity of MnO_2 and low accessible surface area, cause its specific capacitance and power characteristics to weaken [4]. To improve the conductivity of MnO_2-based electrode, the MnO_2 supported with low-dimensional carbon nanomaterials (such as carbon nanotubes, CNTs) was employed for pseudocapacitor applications by enhancing the specific capacitances [5,6]. Herein, the MnO_2 provides high energy density, while the CNTs interconnected network provides a fast pathway for ion and electron transport during charge/discharge process. Recently, graphene, a new carbon material, has been studied as a supporting material to improve the electrochemical performance of MnO_2 due

* Corresponding author.
E-mail address: tseng@cc.nctu.edu.tw (T.Y. Tseng).

0378-7753/$ – see front matter © 2013 Elsevier B.V. All rights reserved.
http://dx.doi.org/10.1016/j.jpowsour.2013.06.055

to the unique structural and electrical properties [7]. Many graphene–MnO_2 nanocomposites as electrode material for lithium-ion battery and pseudocapacitor have been investigated in recent years. However, pseudocapacitive properties of MnO_2 nanocomposites grown on carbon material (e.g., CNTs or graphene) are limited. It attributed to the decrease of conductivity of the electrode, due to the breaking of the carbon conductive porous network structure by MnO_2 coating [8]. In addition, re-stacking of graphene sheets into graphite also reduced the effective surface area leading to decrease of the overall conductivity of graphene [9]. Up to now, only a few papers are reported to prevent the agglomeration and re-stacking behavior of graphene-based nanocomposites. Wang et al. utilized a hydrothermal method to fabricate the 3-D hierarchical structure of graphene using CNTs as the spacer between the graphene sheets that have a high specific capacitance of 318 F g^{-1} [10]. Cheng et al. utilized a vacuum filtration method to fabricate superior conductive film based on the interconnected nanocomposites mixed of graphene/MnO_2 composite and CNTs for pseudocapacitor electrode to have a specific capacitance of 372 F g^{-1} [8]. Therefore, it is an important goal to develop a novel process for fabricating excellent graphene-based nanocomposites electrode for energy storage application. Based on above experience, the efficient way to avoid agglomeration and re-stacking behavior of graphene sheets into graphite is to employ a suitable nano-spacer inserted into graphene. Moreover, the nano-spacer requires increasing the overall surface area and conductivity of the graphene-based material on pseudocapacitor.

Up to now, many works focus on graphene-based nanocomposites electrode with binder enrichment for pseudocapacitor application; however, the binder (polymer) is regarded as high charge-transfer resistance material. It would decrease charge/electron transport between the current collector and the active electrode materials, which make pseudocapacitor reduce the performance and efficiency. According to our previous study, the nanocomposites pseudocapacitor electrode was fabricated by electrophoretic deposition (EPD) without adding any binder or surfactants, which is regard as a simple way to solve this issue [6].

As compared to other fabrication methods (e.g., paste/press method, slurry method and vacuum filtration method) on the pseudocapacitor electrodes, EPD offers the several significant advantages of a non-vacuum method, room-temperature processing, short processing time, low cost, scalable, additive free and suitability for mass production. In addition, it can also offer the mass of the deposited particles control, namely, the thickness of the films can be easily controlled by the concentration of the suspension, applied potential, and deposition time. Regarding the engineering feasibility study, EPD method is the most feasible option for the practical application of pseudocapacitor. However, there is very limited literature that has ever been reported on the fabrication of graphene/CNTs/MnO_2 nanocomposites (in short, GMC) pseudocapacitor electrode by EPD method.

In this paper, we focus on the hybrid nanocomposite design based on CNTs/MnO_2 nanocomposites (in short, CM), graphene/MnO_2 nanocomposites (in short, GM), GMC, graphene/MnO_2 nanocomposites + CNTs (in short, GM + C), and GMC + C which provide a synergistic improvement on electrochemical performance and stability for pseudocapacitor. The designed hybrid nanocomposites electrodes are fabricated by a modified EPD method using hydrogen ion instead of polymer as surfactant to ionize the surface of nanocomposites to obtain the binder-free electrode for pseudocapacitor. In addition, the MnO_2-based nanocomposites (e.g., CM, GM, and GMC) are synthesized by redox titration method at room temperature. The designed GMC + C electrode with highly nanoporous framework surface structure exhibits a high specific capacitance of 481 F g^{-1} at 5 mV s^{-1} and excellent cycle stability of 83.3% capacitance retention over 15,000 cycles. The excellent pseudocapacitance of designed hybrid nanocomposites electrode implies that CNTs play a critical role in enhancing electrochemical properties, which acts as a spacer to prevent the re-stacking of individual GMC nanocomposites sheets.

2. Experimental

The designed hybrid nanocomposites for pseudocapacitor electrode material was directly deposited onto 10 mm × 30 mm × 1 mm flat Ni substrates by EPD method in this study. The Ni substrate was etched with 10% nitric acid solution for 30 min to obtain rough surface and cleaned with deionized (DI) water in an ultrasonic bath, and dried in an oven at 100 °C for 12 h. The commercial CNTs (specific surface area: 40–300 m^2 g^{-1}, length: 5–20 μm) was purified by boiling at 70% nitric acid solution for 24 h, cleaned by DI water and followed by dried in an oven at 100 °C for 12 h before synthesizing nanocomposites.

2.1. Synthesis of graphene

Graphene was synthesized by reducing the graphene oxide synthesized from natural graphite fine powder (no. 15553, Riedel-de Haën) by a modified Hummers method, reported by Cheng et al. [11]. In a typical synthesis, the graphite power (3.0 g) was added into the concentrated H_2SO_4 (98%, 100 mL) solution with stirring in which $NaNO_3$ (1.5 g) was dissolved at 80 °C and then the suspension was kept under a vacuum environment for 1 h. The resulting product, pre-oxidized graphite, was obtained via filtering the suspension and cleaned by DI water and dried in an oven at 110 °C for 12 h. Then, it was dispersed into H_2SO_4 (98%, 100 mL) in a flask by using ultrasonication. Subsequently, $KMnO_4$ (10 g) powder was added gradually to the suspension under stirring to avoid strong oxidizing reaction. The above suspension was then stirred to react at room temperature for 2 h and would become dark brown slurry. Then, DI water (100 mL) was added into the flask to obtain a light brown suspension. The diluted suspension was stirred at 98 °C for 12 h and H_2O_2 (30%, 30 mL) was added slowly to the diluted suspension and solution color turned into brilliant yellow along with bubbling. The suspension was allowed to aging overnight; the supernatant fluid was decanted and discarded. The remaining product was then cleaned with HCl (5%) solution and deionized water for several times by ultrasonication. The cleaning process was repeated until the pH of the solution became neutral. Finally, the resulting suspension was centrifuged (8000 rpm for 15 min), the supernatant decanted away and dried in an oven at 110 °C for 12 h to obtain the black solid product, graphene oxide.

The as-synthesized graphene oxide (100 mg) was first put in the DI water (50 mL) and dispersed by ultrasonic agitation for 30 min. Then, hydrazine (35% in water, 3 mL) was added to homogeneous graphene oxide dispersion in a flask with stirring at 90 °C for 12 h. After the solution cooled down to room temperature, the as-synthesized product of the reacting solution was collected and then centrifuged and rinsed with DI water several times to remove the excess hydrazine and the ions of the MnO_2 nanoparticles. Finally, the obtained product, graphene was dried in air at 110 °C for overnight.

2.2. Synthesis of GMC nanocomposites

Pseudocapacitor electrode material, GMC nanocomposite powders were synthesized from redox titration method at room temperature. Purified CNTs and graphene were put together in the DI water (50 mL) and dispersed by ultrasonic agitation for 30 min. Then 0.005 M $KMnO_4$ was added into the homogeneous graphene/

CNTs dispersion drop by drop at room temperature. Such a mixture was kept stirred for 6 h until the purple color disappeared. Finally, the nanocomposites were obtained via filtering the solution and rinsed by DI water and dried in an oven at 110 °C for 12 h. For comparison, CM and GM were synthesized via a similar procedure, respectively.

Then, the CM, GM, and GMC nanocomposites film were deposited on the Ni substrate via EPD method, respectively. The electrolyte used in EPD was a mixture of 0.1 g nanocomposites powders (e.g., CM, GM, and GMC) and hydrochloric acid (37%, 0.2 mL) in the isopropyl alcohol (80 mL). The powders were dispersed well in the solution by ultrasonic agitation for 30 min. Nickel and platinum foils were dipped in this solution as a cathode and anode at a distance of 1 cm, respectively. The nanocomposites powders were electrophoretically deposited on the Ni substrate at a 50 V direct current (DC) voltage for 2 min. After EPD, the nanocomposites film formed on Ni substrate was dried in an oven at 110 °C for 12 h which is an as-grown nanocomposites electrode.

For comparison, the hybrid structure of nanocomposites (e.g., GM or GMC) and purified CNTs were synthesized. The electrolyte used in EPD was a mixture of 0.095 g nanocomposites powders (e.g., GM or GMC), 0.005 g CNTs powders (5 wt%), and hydrochloric acid (37%, 0.2 mL) in the isopropyl alcohol (80 mL). Powders were dispersed well in the solution by ultrasonic agitation for 30 min. The hybrid nanocomposites structures were deposited via a similar EPD procedure. After EPD of the hybrid nanocomposites structure film, labeled respectively as GM + C and GMC + C, were dried in an oven at 110 °C for 12 h. Finally, the mass of every as-deposited sample was measured by a high precision microbalance (PRECISA XR125SM-FR) with an accuracy of 1 μg. The loading of all the nanocomposites on Ni substrate was about 90.36 ± 3.5 μg. Table 1 summarizes the composition (wt %) and nomenclature of the nanocomposites prepared.

Field emission scanning electron microscope (FE-SEM, JEOL JSM-6700) and X-ray diffractometer (XRD, Bede D1) were used to analyze surface morphology and crystallization of the film, respectively. The oxidation states of manganese oxide film were examined by X-ray photoelectron spectroscopy (XPS, ULVAC-PHI Quantera SXM). Field emission transmission electron microscope and EDS analysis (FE-TEM, JEOL JEM-2100F) were used to observe the coaxial structure of nanocomposite material. The specific surface area of the nanocomposite material was determined by BET (Brunauer, Emmett and Teller theory) surface area analyzer (ASAP 2020). Raman spectra of nanocomposite material were recorded using a high-resolution confocal Raman microscope (HOROBA, Lab RAM HR). The laser excitation was provided by a regular model laser operating at 632.8 nm. The thermal analysis was performed from 50 to 950 °C at 3 °C min^{-1} ramping rate under air atmosphere using thermogravimetric analyzer (TGA, TA Instruments Q500).

The electrochemical performances of the pseudocapacitors were measured by cyclic voltammetry (CV), galvanostatic charge/discharge cycling (CC) and electrochemical impedance spectroscopy (EIS) using CH Instruments 618B electrochemical analyzer.

Table 1
Mass and composition (wt %) of the nanocomposites.

Nanocomposite	Mass of MnO_2 (mg)	Mass of CNTs (mg)	MnO_2/CNTs weight fraction (wt%)
CM	0.031	0.056	33.0/59.9
GM	0.034	0.044	39.1/51.4
GMC	0.038	0.045	41.2/49.5
GM + C	0.033	0.047	37.6/53.9
GMC + C	0.036	0.048	39.6/53.4

Electrochemical measurements were carried out in a three-electrode cell with a saturated calomel reference electrode (SCE), a counter electrode of platinum sheet, and 0.1 M Na_2SO_4 as the electrolyte. The CV testing was recorded between 0 and 0.8 V versus SCE at a scan rate varied from 5 to 300 mV s^{-1}. The CC testing was recorded between 0 and 0.8 V versus SCE at a current density varied from 3 to 90 A g^{-1}. Value of the specific capacitance (F g^{-1}) was estimated from cyclic voltammetric curve using following equation:

$$C = \frac{\int I\,dt}{\Delta E \times m} \quad (1)$$

where I is the oxidation or reduction current; dt, time differential; m, the mass of the active material; and ΔE, the width of the potential window. For the values of the specific capacitance (F g^{-1}) from galvanostatic charge/discharge cycling curve, the calculation equation is:

$$C = \frac{I\Delta t}{\Delta E \times m} \quad (2)$$

where I is the discharge current; Δt, the time for a full discharge; m, the mass of the active material; and ΔE, the width of the potential window for a full discharge.

Impedance spectroscopy investigation was performed in the frequency range of 0.1 Hz–100 KHz at an open circuit voltage with AC amplitude of 5 mV.

3. Results and discussion

The microstructural images of graphene, GMC, and GMC + C nanocomposites are shown in Fig. 1. Typical top-view FE-SEM surface morphology of the graphene synthesized by a modified Hummers method is shown in Fig. 1a, indicating that a highly porous wrinkling structure electrophoretically deposited on the Ni substrate. TEM analysis was performed on the as-synthesized graphene nanosheets to identify their nanostructure. Fig. 1b shows the TEM image of graphene sheets from the dispersion in ethanol to form a covering on the top of the copper grid. In this case, the two-dimensional (2D) nanosheets extending its sizes in the range of several tens to several hundreds of square nanometres. There are a few layer graphene sheets overlapped shown on the right side of the diagram, and some large area corrugated and thin graphene nanosheets on the left side of the diagram. The heterostructure surface morphology of the GMC nanocomposites is shown in Fig. 1c. It can be observed from the low magnification that the nanocomposites still retain porous wrinkling structure. When examined at a higher resolution, the surface of the nanocomposites is observed much rougher, indicative of the growth of MnO_2 on the graphene/CNTs hybrid material network structure surface, as clearly shown in the inset of Fig. 1c. The morphology can be evidenced by TEM observation which can clearly see the flake-like coating of MnO_2 on the graphene/CNTs matrix surface, as shown in Fig. 1d. Fig. 1e gives the high-resolution TEM (HR-TEM) image of the GMC nanocomposites, and it clearly shows the coating, MnO_2 thickness about less than 10 nm. The corresponding EDS spectrum of the coating indicates the coating is only composed of two elements, namely, Mn and O, as clearly shown in the inset of Fig. 1e. In addition, the appearance of K peaks in the sample indicates K^+ co-existing in the MnO_2 matrix, arising from the precursors, $KMnO_4$, which always happens during the synthesis process of MnO_2 [12,13]. In our experiment, the GMC nanocomposites are formed by redox titration deposition of MnO_2 onto graphene/CNTs hybrid

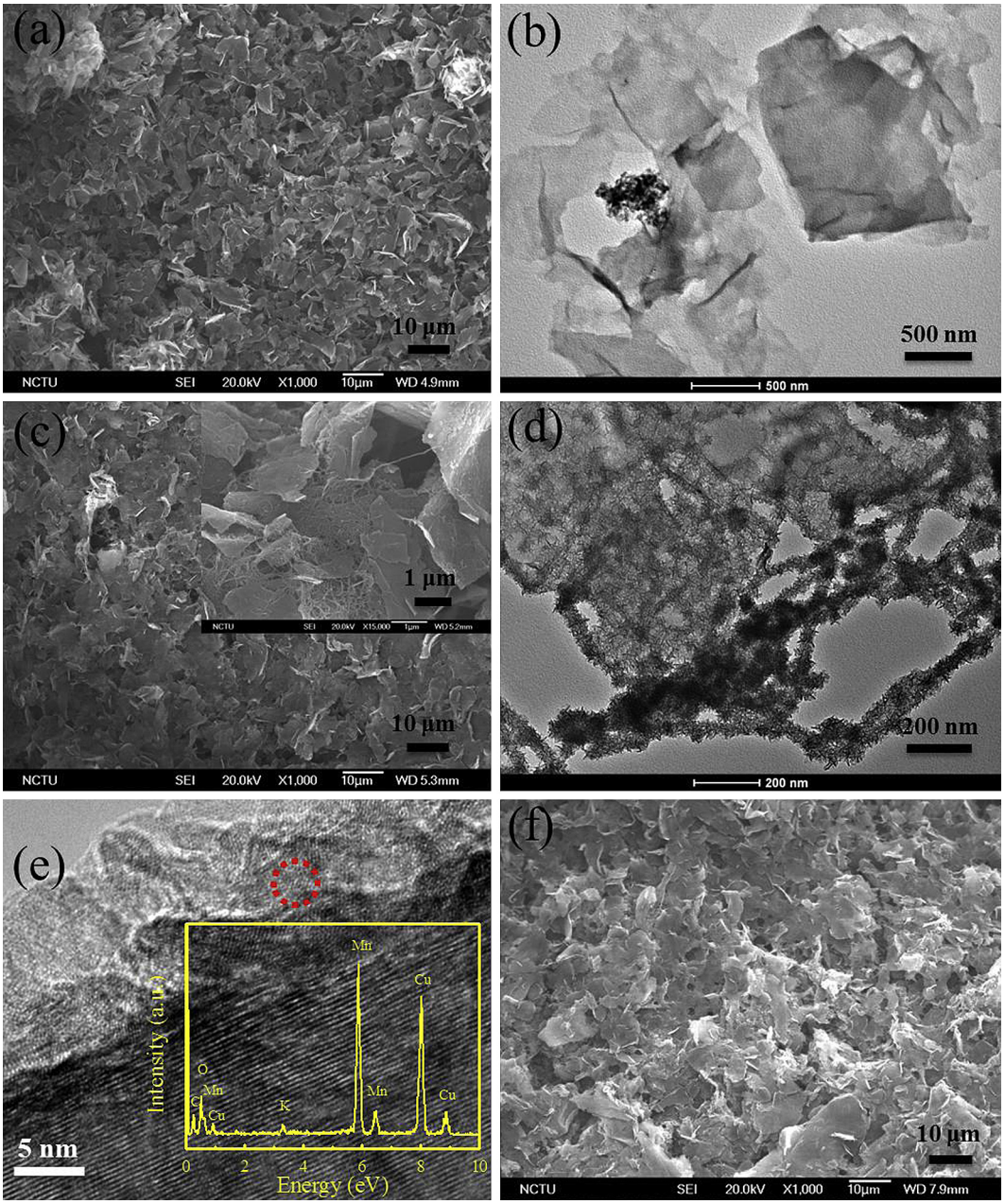

Fig. 1. (a) SEM image and (b) TEM image of the as-synthesized graphene, (c) SEM image (the inset is high-magnification image), (d) TEM image and (e) HR-TEM image (the inset is corresponding EDS pattern of selected part) of GMC nanocomposites, and (f) SEM image of the deigned GMC + C nanocomposites.

material network structure surface at room temperature. The reactions can be explained as follows:

$$4MnO_4^- + 3C + H_2O \rightleftarrows 4MnO_2 + CO_3^{2-} + 2HCO_3^- \quad (3)$$

In reaction (3), it is expected that carbon atom in the surface defect region of the graphene/CNTs hybrid material matrix would react with MnO_4^- ions (from $KMnO_4$) to form Mn(IV) oxide [14]. The GMC and GMC + C nanocomposites exhibit relative highly interconnected porous structure, which ensures larger available surface area to provide a large redox reaction area, as shown in Fig. 1c and f.

Fig. 2a shows the nitrogen adsorption/desorption isotherm of the GMC nanocomposites. The isotherm exhibits a significant hysteresis loop, indicating the existence of mesopores formed between the particles. The specific surface area of the GMC nanocomposites exhibits as high as 197 $m^2\ g^{-1}$, and the pores of sizes are between 19.7 and 179.1 Å with an average pore size of 66.1 Å (as shown in the inset of Fig. 2a), which is much higher than that of MnO_2 synthesized by other methods [14,15].

The TGA curve was used to determine the actual fraction of MnO_2 in the as-synthesized GMC nanocomposites. Data were recorded in air atmosphere at a ramp rate of 3 °C min^{-1} from 50 to 950 °C. From the TGA curve of Fig. 2b, 5% weight loss is observed between 50 and 180 °C, attributed to the removal of surface-adsorbed water, and the 4.3% weight loss between 180 and 390 °C corresponds to the release of adsorbed water in the lattice [16]. The additional weight loss of 41.2% between 390 and 550 °C corresponds to the removal of graphene/CNTs hybrid material. Furthermore, the final weight loss of ~1.6% between 860 and 910 °C is associated with the conversion of MnO_2 to Mn_3O_4 [17].

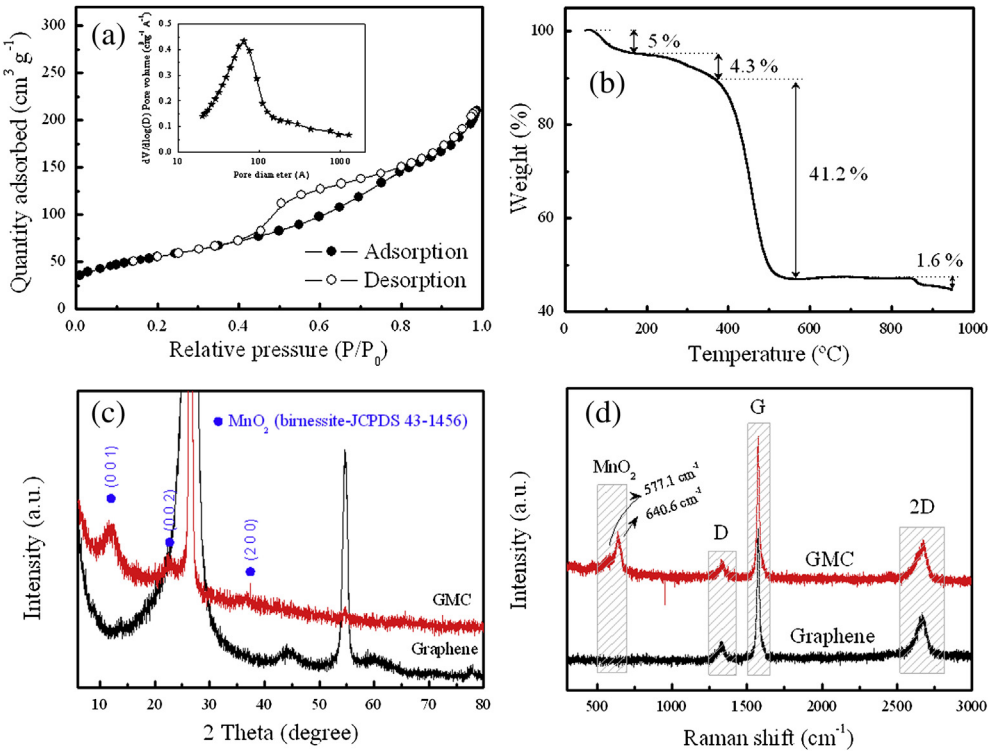

Fig. 2. (a) N_2 adsorption–desorption isotherm, and (b) TGA curve of the deigned GMC nanocomposites, (c) XRD, and (d) Raman analysis of the as-synthesized graphene (lower line) and GMC nanocomposites (upper line).

Thus, the actual fraction of MnO_2 and graphene/CNTs hybrid material matrix in the initial GMC nanocomposites is 49.5% and 41.2%, respectively.

Fig. 2c shows XRD patterns of graphene sheets, and GMC nanocomposites products. After the chemical reduction of graphene oxide, the major peak at 2θ around 26.5° (002) is observed for graphene. In addition, the other two abnormal diffraction peaks at 54.5° (004), and 44.6° (101) are corresponded to the unreacted residual graphite powder. Moreover, the three characteristic peaks of GMC nanocomposites at 12.3° (001), 24.9° (002), and 35.6° (200) can be indexed to birnessite-type MnO_2 (JCPDS 43-1456). From XRD analysis, the wide and broad diffraction peaks demonstrate that the flake-like coating of MnO_2 on the graphene/CNTs matrix surface exhibits a poorly crystallized compound. It has been shown in the previous paper that the better electrochemical performance was obtained for the pseudocapacitor with MnO_2-based electrode containing higher amount of poorly crystallized compound [18] or birnessite-type phase [19]. The poorly crystallized or birnessite-type structure has large interlayer distance and pore volume. The proton and cation of the electrolyte are inserted into this matrix easily, leads to the increase of the reaction area between electrolyte and active electrode materials.

Raman spectroscopy has been used to investigate the vibrational properties of the as-synthesized product. Fig. 2d shows the Raman spectrum of graphene and GMC nanocomposites. It can be clearly observed that there are three peaks containing 2D, G, and D bands at 2569.1, 1574.6, and 1331.3 cm^{-1} in both samples, respectively. The D band exists in the Raman spectrum of the as-synthesized graphene which is likely caused by the defect and disorder carbon corresponding to the unavoidable oxidation by H_2SO_4 and $KMnO_4$ for chemical exfoliation. In the previous works, the 2D/G ratio between the 2D and G peak areas can be used to determine the degree of graphitization for sp^2 (C=C bonds) of graphitic materials and the thickness of graphene layers [20]. The 2D/G ratio is approximately 0.3 for as-synthesized graphene, demonstrating that the thickness of graphene about 15 layers. Meanwhile, for the Raman spectrum of the GMC nanocomposites, the appearance of the weak peaks located at 577.1 and 640.6 cm^{-1}, which can be attributed to the Mn–O lattice vibration, also confirm the evidence for the presence of MnO_2 [21].

XPS was carried out to understand the detailed surface chemical composition of as-synthesized graphene and GMC nanocomposites, and the corresponding results are shown in Fig. 3. Fig. 3a shows the XPS wide survey spectrum of as-synthesized graphene, confirms the presence of carbon and oxygen species. In contrast to GMC nanocomposites, there is a Mn 2*p* signal in XPS wide survey spectrum of GMC, indicating that the evidence for the MnO_2 deposited on the graphene/CNTs hybrid material surface. Fig. 3b shows the Mn 2*p* spectrum of GMC nanocomposites, indicating that there are doublet peaks of Mn $2p_{3/2}$ and Mn $2p_{1/2}$ located at 641.7 and 653.3 eV, respectively, with an energy separation of 11.6 eV. It indicates that the existence of MnO_2 on the grapheme/CNTs hybrid materials, which is in agreement with previously reported data, revealing that the oxidation state of Mn is +4 [22].

Fig. 3c shows the O 1*s* deconvolution spectrum of as-synthesized graphene and GMC nanocomposites by curve fitting. For as-synthesized graphene, the O 1*s* spectrum is deconvoluted into two sub-peaks located at 532.03 and 530.81 eV corresponding to C–O and C=O bonds, respectively. Compared with as-synthesized graphene, the O 1*s* spectrum of GMC nanocomposites reveals the presence of three components, namely, Mn–O–Mn (529.4 eV), Mn–O–H (530.9 eV), and adsorbed water, H_2O_{ads} (532.3 eV), which are all in agreement with reported results [23,24]. Moreover, Fig. 3d shows the C 1*s* deconvolution spectrum of as-synthesized graphene and GMC nanocomposites through the process of curve fitting. For as-synthesized graphene, deconvolution of C 1*s* spectrum produces 4 main peaks around 283.9, 285.05, 286.56, and 288.4 eV assigned to

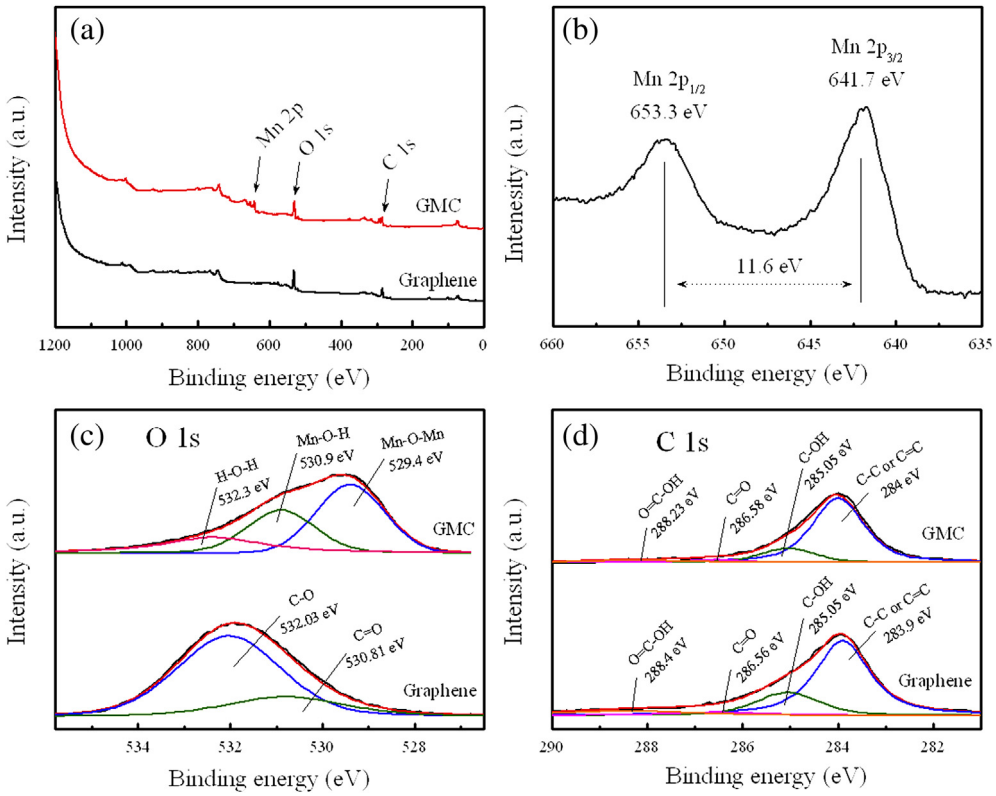

Fig. 3. (a) Wide XPS survey spectra of the as-synthesized graphene (lower line) and deigned GMC nanocomposites (upper line), (b) Mn 2*p* spectra of the GMC nanocomposites, (c) XPS O 1*s* spectra and (d) XPS C 1*s* of the as-synthesized graphene and GMC nanocomposites.

C═C/C–C, C–OH (hydroxyl and epoxy groups), C═O (carboxyl groups) and O═C–OH (carboxylate groups) bonds, respectively. Compared with as-synthesized graphene, the C 1*s* spectrum of GMC nanocomposites shows the same functional groups. But with lower concentration of the oxygenated carbon, it indicates that growth of MnO_2 on the surface of graphene/CNTs hybrid material under the slow oxidation process, which is the interaction between MnO_4^- and oxygenated carbon group [25].

The CV, CC, and EIS measurements were employed to understand the capacitive behavior of the as-prepared pseudocapacitor electrodes. Fig. 4a shows the typical CV curves of the CM, GM, GMC, GM + C, and GMC + C electrodes in neutral aqueous electrolyte (0.1 M Na_2SO_4) at 25 °C in the potential in the range $0 < E_{SCE} < 0.8$ V versus SCE at a scan rate of 100 mV s^{-1}. It is obvious that all of the typical CV curves for the different hybrid structures of nanocomposite electrodes are almost a near-ideal rectangular and symmetric profile and no redox peaks appear in the cycling from 0 to 0.8 V, indicative of a typical capacitor-like behavior. Thus, according to Eq. (1), the variation of measured specific capacitances of nanocomposites with different hybrid structures is indicated in the inset of Fig. 4a. The calculated specific capacitances of CM, GM, GMC, GM + C, and GMC + C electrodes at 100 mV s^{-1} are 117, 210, 278, 188, and 398 F g^{-1}, respectively. For all the pseudocapacitor electrodes, the GMC + C hybrid nanocomposite electrode shows best performance among the five electrode materials.

In comparison with the CV results, Fig. 4b shows the charge/discharge (CC) curves for all hybrid nanocomposite electrodes in neutral aqueous electrolyte (0.1 M Na_2SO_4) at 25 °C in the range $0 < E_{SCE} < 0.8$ V versus SCE at the same current density of 3 A g^{-1}. All of the typical CC curves for all hybrid structures of nanocomposite electrode show ideal capacitive behavior in terms of the linear and symmetric characteristics with a constant slope in the range of operating potential, reflecting the excellent storage capability. In addition, the internal resistance (IR drop) in CC curves can also be investigated. It is clearly seen that the GMC + C electrode displays much smaller IR drop (~6.5 Ω) than the other electrodes at a given current density, as seen from the inset of Fig. 4b. According to Eq. (2), the specific capacitance of GMC + C electrode at current density of 3 A g^{-1} is 416 F g^{-1}, which is higher than those of CM (123 F g^{-1}), GM (260 F g^{-1}), GMC (353 F g^{-1}), and GM + C electrode (216 F g^{-1}), which are plotted in the inset of Fig. 4b. The values of specific capacitances obtained from CV and CC curves are little difference, but the trends are identical.

Effect of the hybrid nanocomposites electrode structure on the electrochemical characteristics can be demonstrated from electrochemical impedance spectroscopy (EIS). The Nyquist plots of the AC impedance responses for those electrodes in 0.1 M Na_2SO_4 electrolyte are shown in Fig. 4c. It is noted that all spectra contain a semicircle in the high frequency region, a straight line inclined at a constant phase in the mid-frequency region, and an almost vertical capacitive line in the low frequency region. The bulk resistance (R_s) of the electrochemical system can be found from the intersection of the semicircle on the real impedance *x*-axis in the range of high frequency, while the diameter of the semicircle corresponds to the charge-transfer resistance (R_{ct}) on the surface of the electrode in contact with the electrolyte. For all of the samples, the GMC + C electrode shows the minimum R_s (~2.1 Ω cm^2) and R_{ct} (~2.63 Ω cm^2), indicating that the interfacial contact between the GMC nanocomposite and the CNTs are the best contact. The designed hybrid nanocomposites structure promotes ion migration within electrode materials, which facilitates efficient utilization of active materials [26].

Besides, from the inset of Fig. 4c, it shows the plot at a medium frequency, the knee-frequency, which is the maximum frequency

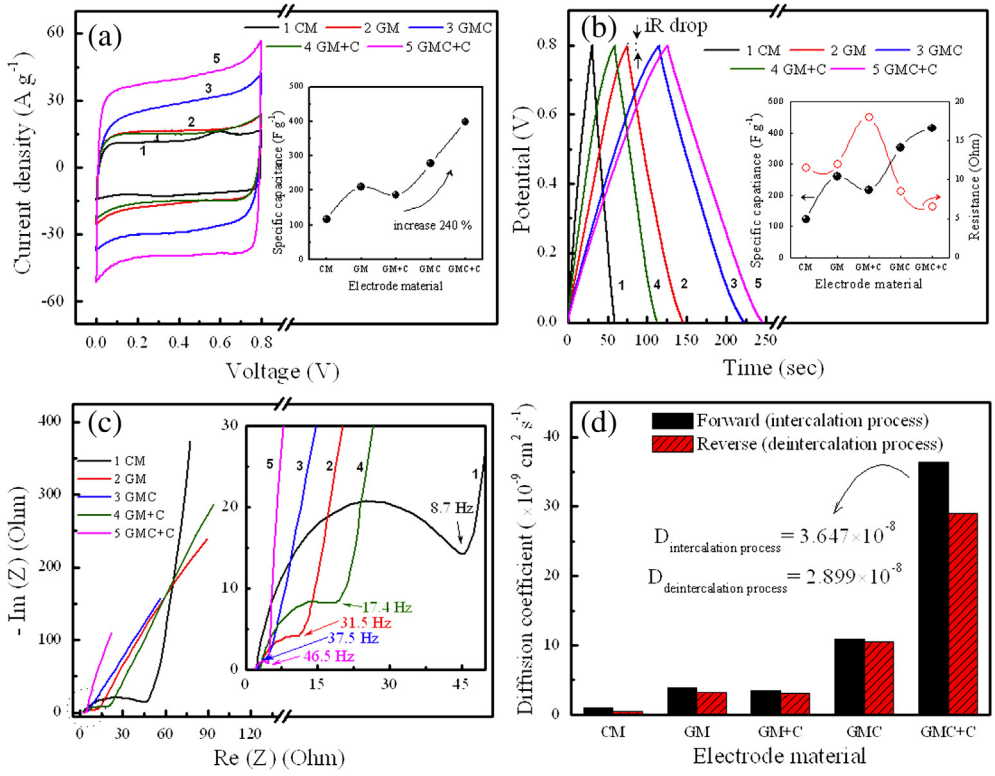

Fig. 4. (a) The CV curves at a scan rate of 100 mV s^{-1}, (b) the CC curves at current density of 3 A g^{-1} (the inset is the specific capacitance of different designed hybrid structures), (c) Nyquist plots (the insets show the enlargement portion of selected part indicated), and (d) the sodium ion diffusion coefficient values for intercalation and deintercalation of the designed CM, GM, GMC, GM + C, and GMC + C electrodes.

where the energy storage starts [27]. For all electrodes, it is obvious that the GMC + C electrode exhibits higher knee-frequency at 46.5 Hz than those of CM (8.7 Hz), GM (31.5 Hz), GMC (37.5 Hz), and GM + C electrode (17.4 Hz). An electrode with a higher knee frequency can be more rapidly charged and discharged [28]. In addition, Warburg impendence related to a combination of the ion diffusion at the interface between the active electrode material and electrolyte which is employed to fit the straight line at a lower frequency range below the knee-frequency. It worth noting that the GMC + C electrode shows the steeper straight line than the others, showing the designed hierarchical structure with the suitable fast pathway for ion and electron transport without kinetic limitations [29]. To further understand the relationship between the mobilities of ions and electrons, Chronoamperometry experiment (CA) was used to measure the diffusion coefficient *D*. The *D* is calculated using following the Cottrell equation [30]:

$$i_t = \frac{nFAC_0D_0^{1/2}}{\pi^{1/2}t^{1/2}} \quad (4)$$

where *n* is stoichiometric number of electrons involved in the reaction; *F*, Faraday's constant (96,485 C mol^{-1}), A the area of the electrode surface (cm^2); C_0, the concentration of electroactive species (mol cm^{-3}), and D_0 the diffusion coefficient (cm^2 s^{-1}).

Fig. 4d shows the diffusion coefficient values for intercalation and deintercalation of Na^+ in the different hybrid structures of nanocomposites electrode in 0.1 M Na_2SO_4. The GMC + C electrode exhibits a higher intercalation value of 3.647 × 10^{-8} cm^2 s^{-1} and a slightly lower deintercalation value of 2.899 × 10^{-8} cm^2 s^{-1}. It is obvious that the GMC + C electrode shows 33, 9, 3, and 10-fold higher diffusion coefficient than those of CM, GM, GMC, and GM + C, respectively, even better than the other reported results [31,32]. Enhancement of ion diffusion into GMC + C electrode can be attributed to the designed hybrid nanostructure. In our system, the graphene/CNTs hybrid matrix with nanoporous framework surface structure serves as the connecter between the MnO_2, which prefers to attach to the defect sites on the graphene/CNTs. The resistance of GMC + C nanocomposites is lowered by the connected CNTs, which provide large specific surface area and short diffusion length. It reveals that fast ions transport can quickly and easily diffused into the storage sites of the stacked layers. It has been well established that the designed GMC + C hybrid nanocomposites electrode exhibits excellent capacitive behavior.

To get more information on the electrochemical behavior and capacitor performance of designed GMC + C hybrid nanocomposites as pseudocapacitor electrode, we performed the detailed measurements of CV, CC, and long-term stability test in a three-electrode configuration. The variation of measured specific capacitances with different scan rates is indicated in Fig. 5a. All the CV curves appear almost a near-ideal symmetric rectangular profile and a rapid current response to voltage reversal at each end potential even at a high scan rate of 300 mV s^{-1}. Mean calculated specific capacitances are 481, 436, 413, 398, and 372 F g^{-1} as a function of different scan rates of 5, 20, 50, 100, and 300 mV s^{-1}, respectively. As shown in Fig. 5c, the specific capacitance at 300 mV s^{-1} of the GMC + C electrode is 77.2% of that measured with 5 mV s^{-1}. These results show excellent power capability behavior and lower equivalent series resistance of the designed GMC + C hybrid structure electrode.

Fig. 5b depicts the charge/discharge behavior of GMC + C electrode between 0 and 0.8 V at various current densities. It is clearly seen that all these CC curves are very symmetric; the slope of every curve is potential independent with a constant value, IR drops of the all curves are potential dependent at various current densities

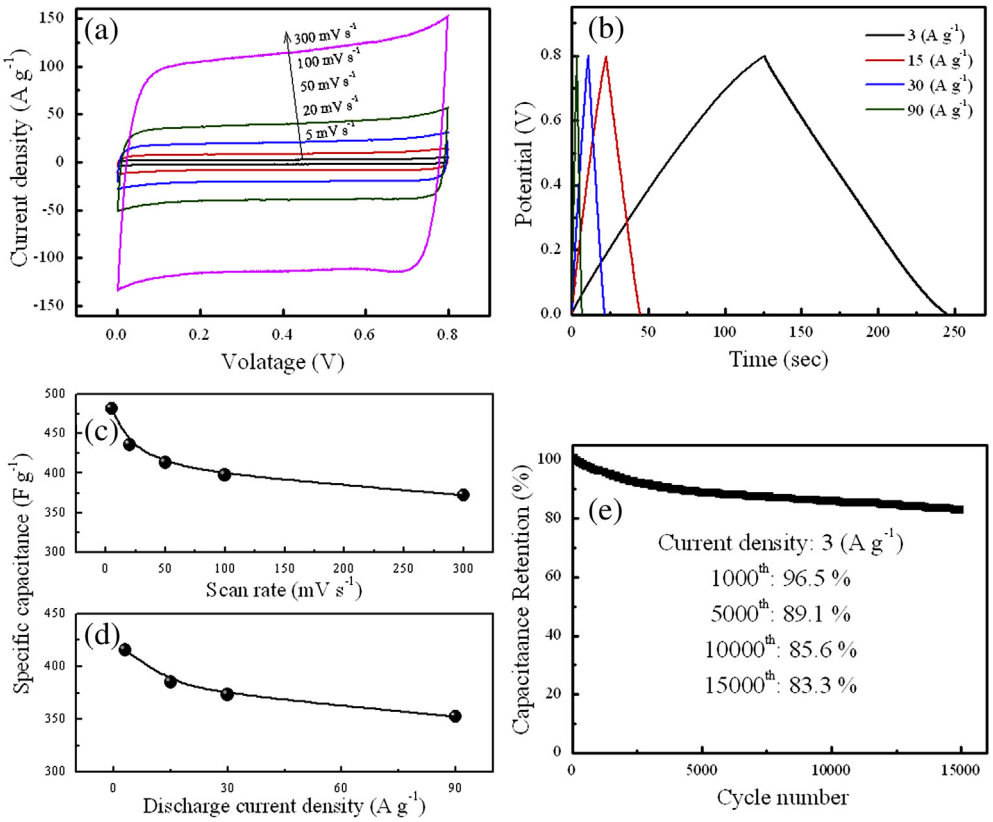

Fig. 5. (a) The CV curves in 0.1 M Na_2SO_4 at scan rates of 5, 20, 50, 100 and 300 mV s^{-1}, (b) the CC curves in 0.1 M Na_2SO_4 at current density of 3, 15, 30, and 90 A g^{-1}, (c) summary plot of specific capacitance from CV curves, (d) summary plot of specific capacitance from CC curves, and (e) the cycling stability (at a constant charge/discharge current density of 3 A g^{-1}) of the deigned GMC + C nanocomposites electrode.

from 3 to 90 A g^{-1}. From the CC curve, the specific capacitance of GMC + C electrode at current densities of 3, 15, 30, and 90 A g^{-1} can be calculated as 416, 385, 373, and 353 F g^{-1}, respectively. Even when the discharge current is enhanced 30 times, from 3 to 90 A g^{-1}, the designed GMC + C electrode can hold 85% retention, which is plotted in Fig. 5d. This further demonstrates that the GMC + C nanocomposites with nanoporous framework surface structure provide large specific surface area and short diffusion length for ion to improve the overall pseudocapacitor performance.

Fig. 5e displays the cycling stability of the GMC + C electrode pseudocapacitor with the 0.1 M Na_2SO_4 electrolyte at a constant charge/discharge current density of 3 A g^{-1}. After 15,000 charge/discharge cycles, the pseudocapacitor maintains a high specific capacitance of 346 F g^{-1}. It is about 83.3% of the initial capacitance (415 F g^{-1}), indicating the excellent cycle durability of the pseudocapacitor. Therefore, owing to the highly nanoporous framework surface structure of the designed GMC + C electrode, it exhibits not only high capacitance but also long cycling stability, essential for practical applications.

It is worth pointing out that, the amount of active material loaded on the current collector is very important for the practical application like battery or pseudocapacitor system. We have explored the relationship between the specific capacitance value and total amount of material deposited on the per substrate area. Specific capacitance versus GMC + C nanocomposites with different mass loadings is plotted in Fig. 6. As the amount of deposited GMC + C nanocomposites and MnO_2 increases, the coating thicknesses per substrate area are increased accordingly. However, the average specific capacitance was nonlinearly decreases. This decrease in capacitance is due to the increasing thickness and decreasing the effective contact reactive surface area between the electrode and electrolyte.

In addition, we also offer the dependence of specific capacitance on mass fraction of CNTs in the GMC + C nanocomposite. As shown in Fig. 7, the specific capacitance is increases until the mass fraction of CNTs are increased up to 5 wt% and then decreases with further increasing of CNTs mass fraction. However, increasing the amount of CNTs improve electronic conductivity of the nanocomposites pseudocapacitor electrode. But, after 5 wt% of CNTs mass fraction,

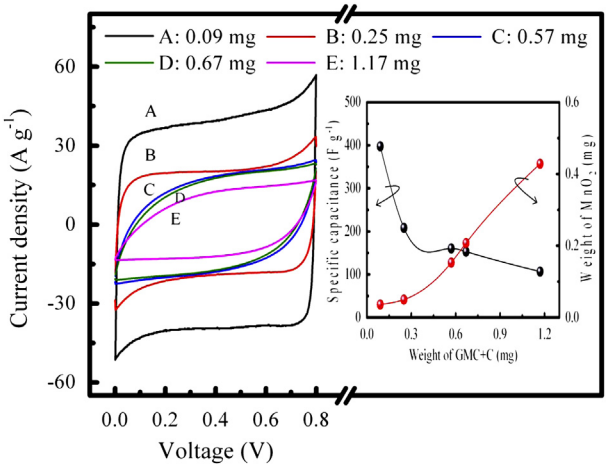

Fig. 6. The CV curves of the electrode as a function of deposited weight of GMC + C nanocomposites in 0.1 M Na_2SO_4 at scan rate 100 mV s^{-1}.

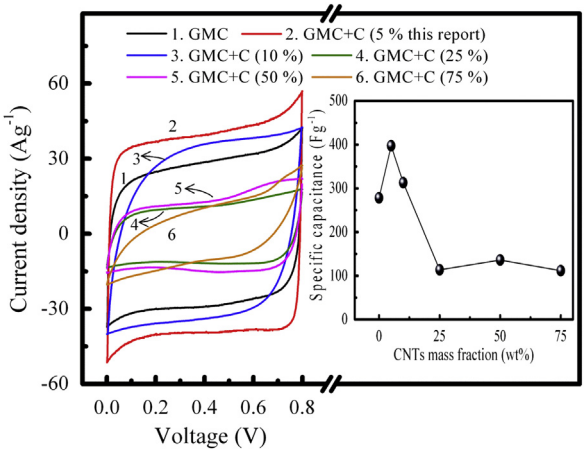

Fig. 7. CV curves in 0.1 M Na_2SO_4 at scan rate 100 mV s^{-1}. Specific capacitance as a function of CNTs mass fraction in the GMC + C nanocomposites (inset).

the reduction of MnO_2 mass fraction in the nanocomposites affects the specific capacitance more severely than the increase of surface area by the CNTs mass fraction [33]. Here, the major role of CNTs is to supply a spacer inserted into the individual GMC nanocomposites to reduce the electrode resistivity. In addition, it evidences that the specific capacitance of the GMC + C based nanocomposites is dominated by the redox reaction of MnO_2. Thus, adding 5 wt% of CNTs and the suitable amount of active material in the GMC + C of Figs. 4 and 5 is identified as the optimum percentage, which gives rise to the best pseudocapacitive performance in this study.

All these designed hybrid nanocomposites electrode with excellent pseudocapacitance is attributed by the CNTs, which plays a critical role in promoting by acting as a spacer to prevent the re-stacking of individual GMC nanocomposites sheets, during charge/discharge process.

4. Conclusions

In summary, hybrid nanocomposites provided a synergistic improvement on electrochemical performance and stability for pseudocapacitor. With the help of the addition of CNTs, it expands the interlayer distance between adjacent graphene or GMC nanosheets to prevent agglomeration and re-stacking behavior. Designed GMC + C electrode with highly nanoporous framework surface structure is fabricated by a modified EPD method. It is regarded as a simple and green route to decrease the charge-transfer resistance and to increase efficient charge/electron transport from the current collector to the active materials. Designed nanocomposites of flake-like MnO_2 uniformly distributed on highly nanoporous framework surface structure proved by BET, XRD, SEM, and TEM study, respectively. The GMC + C electrode shows the best electrochemical performance among the five electrode materials (CM, GM, GMC, GM + C, and GMC + C). In addition, the sodium ion diffusion coefficients of the GMC + C electrode shows a higher intercalation value of 3.647×10^{-8} cm^2 s^{-1} and deintercalation value of 2.899×10^{-8} cm^2 s^{-1}, attributing to highly nanoporous framework surface structure regarded as a fast ion transport path. Besides, the GMC + C electrode exhibits a high specific capacitance of 346 F g^{-1}, which is about 83.3% of the initial capacitance (415 F g^{-1}) after 15,000 charge/discharge cycles, indicating the excellent cycle durability of the pseudocapacitor. Our designed hybrid GMC + C nanocomposites pseudocapacitor electrode using EPD exhibits high specific capacitance, fast reaction rate, and high stability, suitable for practical applications.

Acknowledgment

This work was supported by the National Science Council of ROC under contract no. NSC 99-2221-E-009-064-MY3.

References

[1] C. Liu, F. Li, L.P. Ma, H.M. Cheng, Adv. Mater. 22 (2010) E28.
[2] X. Zhao, B.M. Sánchez, P.J. Dobson, P.S. Grant, Nanoscale 3 (2011) 839.
[3] M. Winter, R.J. Brodd, Chem. Rev. 104 (2004) 4245.
[4] W. Wei, X. Cui, W. Chena, D.G. Ivey, Chem. Soc. Rev. 40 (2011) 1697.
[5] C.Y. Lee, H.M. Tsai, H.J. Chuang, S.Y. Li, P. Lin, T.Y. Tseng, J. Electrochem. Soc. 152 (2005) A716.
[6] C.J. Hung, J.H. Hung, P. Lin, T.Y. Tseng, J. Electrochem. Soc. 158 (2011) A942.
[7] Y. Sun, Q. Wu, G. Shi, Energy Environ. Sci. 4 (2011) 1113.
[8] Y. Cheng, S. Lu, H. Zhang, C.V. Varanasi, J. Liu, Nano Lett. 12 (2012) 4206.
[9] X. Wang, L. Zhi, K. Müllen, Nano Lett. 8 (2008) 323.
[10] Y. Wang, Y. Wu, Y. Huang, F. Zhang, X. Yang, Y. Ma, Y. Chen, J. Phys. Chem. C 115 (2011) 23192.
[11] Q. Cheng, J. Tang, J. Ma, H. Zhang, N. Shinya, L.C. Qin, Carbon 49 (2011) 2917.
[12] H.Q. Wang, G. f. Yang, Q.Y. Li, X.X. Zhong, F.P. Wang, Z.S. Li, Y. h. Lic, New J. Chem. 35 (2011) 469.
[13] Z. Li, J. Wang, S. Liu, X. Liu, S. Yang, J. Power Sources 196 (2011) 8160.
[14] G. Zhao, J. Li, L. Jiang, H. Dong, X. Wang, W. Hu, Chem. Sci. 3 (2012) 433.
[15] Q. Cheng, J. Tang, J. Ma, H. Zhang, N. Shinya, L.C. Qin, Phys. Chem. Chem. Phys. 13 (2011) 17615.
[16] J. Zhu, J. He, ACS Appl. Mater. Interfaces 4 (2012) 1770.
[17] J. Li, N. Wang, Y. Zhao, Y. Ding, L. Guan, Electrochem. Commun. 13 (2011) 698.
[18] H.Y. Chu, Q.Y. Lai, L. Wang, J.F. Lu, Y. Zhao, Ionics 16 (2010) 233.
[19] O. Ghodbane, J.L. Pascal, F. Favier, ACS Appl. Mater. Interfaces 1 (2009) 1130.
[20] Z. Ni, Y. Wang, T. Yu, Z. Shen, Nano Res. 1 (2008) 273.
[21] C. Zhu, S. Guo, Y. Fang, L. Han, E. Wang, S. Dong, Nano Res. 4 (2011) 648.
[22] H. Huang, X. Wang, Nanoscale 3 (2011) 3185.
[23] H.W. Nesbitt, D. Banerjee, Am. Miner. 83 (1998) 305.
[24] S.C. Pang, M.A. Anderson, J. Mater. Res. 15 (2000) 2096.
[25] Y. Chen, Y. Zhang, D. Geng, R. Li, H. Hong, J. Chen, X. Sun, Carbon 49 (2011) 4434.
[26] H. Chen, S. Zhou, M. Chen, L. Wu, J. Mater. Chem. 22 (2012) 25207.
[27] B.G. Choi, Y.S. Huh, W.H. Hong, H.J. Kim, H.S. Park, Nanoscale 4 (2012) 5394.
[28] C. Du, N. Pan, J. Power Sources 160 (2006) 1487.
[29] R.B. Rakhi, W. C., D. Cha, H.N. Alshareef, Nano Lett. 12 (2012) 2559.
[30] A.J. Bard, G. Inzelt, F. Scholz, in: Electrochemical Dictionary, second ed., Springer, 2012, p. 130.
[31] M.N. Patel, X. Wang, B. Wilson, D.A. Ferrer, S. Dai, K.J. Stevenson, K.P. Johnston, J. Mater. Chem. 20 (2010) 390.
[32] M.N. Patel, X. Wang, D.A. Slanac, D.A. Ferrer, S. Dai, K.P. Johnston, K.J. Stevenson, J. Mater. Chem. 22 (2012) 3160.
[33] J.Y. Lee, K. Liang, K.H. Ana, Y.H. Lee, Synth. Met. 150 (2005) 153–157.